Electronic Supplementary Material (ESI) for Energy & Environmental Science.

Supporting information

Deciphering the High Overpotential of Oxygen Reduction Reaction via Comprehensively Elucidating the Open Circuit Potential

Zenan Wu, Guangxing Yang,* Zhiting Liu,* Qiao Zhang, and Feng Peng*

School of Chemistry and Chemical Engineering, Guangzhou University, Guangzhou 510006, China

Corresponding authors: G. Yang (yanggx@gzhu.edu.cn), Z. Liu (liuzt@gzhu.edu.cn), F. Peng (fpeng@gzhu.edu.cn)

This PDF file includes:

Supplementary text

Methods

Materials

Pt/C (20 wt%, Johnson Matthey); Deionized water (Milli-Q water system, 18.2 MΩ·cm); D_2O, (99.9 at.% D, Shanghai Aladdin Biochemical Technology Co., Ltd); $HClO_4$ (72%, Shanghai Aladdin Biochemical Technology Co., Ltd); H_2SO_4 (GR, Guangzhou Chemistry Reagent Factory); D_2SO_4 (90 wt% in D_2O, Shanghai Macklin Biochemical Technology Co., Ltd); Ar, O_2 and H_2 cylinder gases (Ultrahigh purity, Foshan MS Messer Gas Co., Ltd); ethanol (GC, Shanghai Aladdin Biochemical Technology Co., Ltd); Nafion solution (5.0 wt%, Du Pont China Holding Co., Ltd.).

Preparation of catalyst inks

As for the preparation of catalyst inks, 4 mg of commercial Pt/C were dispersed in a 2 mL solution composed of DI water (0.2 mL), ethanol (1.8 mL), and 5.0 wt% Nafion solution (12 μL), followed by ultrasonication in an ice bath for 30 min. 12.38 μL of the catalyst ink was dropped onto the glassy carbon to give a Pt loading of 20 $\mu g_{Pt}\ cm^{-2}$ and further dried under rotating conditions at room temperature. The catalyst ink should be preserved in a sealed container and refrigerated after use to avoid solvent evaporation, which may alter the consistency of the catalyst loading in each application.

Electrochemical tests

The electrochemical cells and all other glassware used in the experiments were soaked in aqua regia overnight and cleaned prior to electrochemical measurements. The glassware was boiled in DI water five times to thoroughly clean the glassware of residual aqua regia and other trace impurities. All electrochemical measurements were conducted at room temperature in the 5-neck flask (volume of 250 mL or 40 mL) with three-electrode by an electrochemical workstation (CHI760e, Shanghai Chenhua Co., Ltd.). A glassy carbon electrode (Area: 0.2475 cm^2, RRDE, Pine Instruments), a Pt foil, and the Hg/Hg_2SO_4 electrode were employed as working electrode, counter electrode, and reference electrode, respectively.

Electrochemical tests in 0.1 M $HClO_4$

A 150 mL solution of 0.1 M $HClO_4$ was transferred into a 250 mL five-necked flask and purged with Ar for 15 min to remove dissolved O_2. The Pt/C catalyst was then subjected to 30 cyclic voltammetry cycles between 0.03-1.1 V vs. RHE at a scan rate of 50 mV s^{-1} to obtain a stable CV curve. The electrolyte was subsequently replaced with fresh electrolyte and purged with Ar for an additional 15 min for further electrochemical tests.

The Open Circuit Potential (OCP) testing was conducted using the electrochemical workstation's OCPT test technique. The OCP-time curve of Pt/C was recorded under various conditions. The effect of different O_2 partial pressures on OCP was examined by initially recording in an O_2-free electrolyte with continuous Ar introduction. Once a stable OCP was achieved (where OCP did not significantly change over time), different O_2 partial pressures were quickly set using volumetric flowmeter pressures (P_{O_2}/P_0 = 1/3, 1/2, 2/3, 1, with a total flow rate of 200 ml min^{-1}), and the OCP change was recorded for approximately 15 minutes at each O_2 partial pressure. For the test regarding the impact of pH on OCP, the electrolyte's pH was controlled by successively adding 500 ul, 1000 ul, 2000 ul, and 4000 ul of 0.1 M $HClO_4$ to 150 ml of deionized water in situ. The OCP changes were recorded for about 10 minutes at each pH under continuous O_2 introduction. The effect of $H_2Pt(OH)_6$ on OCP was examined by first recording the OCP-time curve of Pt/C in the O_2-free electrolyte while Ar was continuously introduced. Upon reaching a stable OCP, pure O_2 was introduced into the electrolyte, and the OCP was continuously recorded until it stabilized. Subsequently, 10 ml of O_2-saturated electrolyte was withdrawn from the electrolytic cell to ultrasonically dissolve 9 mg of $H_2Pt(OH)_6$, which was then added to the electrolyte in situ using a pipette gun to record the OCP until stabilization. Conversely, in the OCP test where $H_2Pt(OH)_6$ was added first and then O_2 was introduced, the OCP-time curve of Pt/C in the O_2-free electrolyte was first recorded while Ar was continuously introduced. Upon reaching a stable OCP, 10 ml of O_2-free electrolyte was withdrawn from the electrolytic cell to dissolve 9 mg of $H_2Pt(OH)_6$ ultrasonically, then added in situ to the electrolyte using a pipette gun to record the OCP until it stabilized. Subsequently, pure O_2 was introduced into the electrolyte and the OCP was continuously recorded until stabilization.

In the LSV test, each parameter was subjected to independent experiments to eliminate the

effect of Pt/C performance decay during the test process. For example, for different upper limit potentials (E_{upl}) and scanning directions, the cathodic polarization curves between 0.07-E_{upl} V vs. RHE (E_{upl} = 0.97, 1.07, 1.17) were recorded in sequence from small to large in O_2-free electrolyte at a scan rate of 10 mV s^{-1} and a rotation rate of 1600 rpm. Then, under the same test conditions (replacing the fresh electrolyte and preparing the working electrode again), the anodic polarization curves between 0.07-Eupl V vs. RHE (E_{upl} = 0.97, 1.07, 1.17) were recorded. The electrolyte was then saturated with O_2 by bulging O_2 for 15 min and the cathodic and anodic polarization curves between 0.07-E_{upl} V vs. RHE (E_{upl} = 0.97, 1.07, 1.17) were recorded sequentially using the same measurement protocol (10 mV s^{-1}, 1600 rpm) (also two independent experiments). For quiet time, cathodic polarization curves for different quiet times (10 s, 20 s, 30 s) were initially recorded in O_2-free electrolyte at a scan rate of 10 mV s^{-1} and a rotation rate of 1600 rpm between 0.07-E_{upl} V vs. RHE (E_{upl} = 0.97, 1.07, 1.17). The electrolyte was then saturated with O_2 by bubbling O_2 for 15 min and cathodic polarization curves for different Quiet times (10 s, 20 s, 30 s) between 0.07-E_{upl} V vs. RHE (E_{upl} = 0.97, 1.07, 1.17) under O_2-saturated conditions were also recorded sequentially using the same measurement protocol (10 mV s^{-1}, 1600 rpm). For scan rates, cathodic and anodic polarization curves between 0.07-1.07 V vs. RHE were initially recorded in O_2-free electrolyte at different scan rates (10 mV s^{-1}, 50 mV s^{-1}, 150 mV s^{-1}) at a rotation rate of 1600 rpm. The electrolyte was then saturated with O_2 by bubbling O_2 for 15 min and cathodic and anodic polarization curves were recorded in the O_2-saturated electrolyte at the same scan rates (10 mV s^{-1}, 50 mV s^{-1}, 150 mV s^{-1}) using the same measurement protocol (0.07-1.07 V vs. RHE, 1600 rpm).

Electrochemical tests in deuterated electrolyte.

A 40 mL five-necked flask was utilized for the tests. A glass carbon electrode (Area: 0.2475 cm^2, RRDE, Pine Instruments), a Pt foil, and the Hg/Hg_2SO_4 electrode were employed as working electrode, counter electrode, and reference electrode, respectively.

In the ORR test, 9 mL of pure 0.5 M D_2SO_4/D_2O was initially added to a clean and dry five-necked flask. The solution was then bubbled with Ar for 15 min to remove O_2 from the solution. The clean and dry flask was used to avoid the influence of trace amounts of H_2O in the initial system. Subsequently, cyclic voltammetry curves of the activated Pt/C (the activation step was similar to that in 0.1 M $HClO_4$) in the potential range of 0.03-1.3 V vs. RHE was recorded at a scan rate of 50

mV s^{-1}. The electrolyte was then saturated with O_2 for 15 min, and polarization curves were recorded for anodic and cathodic scans, respectively, at 1600 rpm in the potential range of 0.08-1 V vs. RHE. After adding an equal volume (9 mL) of 0.5 M H_2SO_4/H_2O to the same system in situ, the same CV and ORR tests were repeated.

In the OCP test, we used the OCPT test technique of the electrochemical workstation to record the OCP-time curve in 9 mL of pure O_2-free 0.5 M D_2SO_4/D_2O, until the OCP did not change significantly with time, then we quickly set different O_2 partial pressures (P_{O_2}/P_0 = 1/3, 1/2, 2/3, 1) by controlling the gas flow rates of Ar and O_2 (with a total flow rate of 200 mL min^{-1}) using a volumetric flowmeter, and recorded the change of OCP for about 10 min under each O_2 partial pressure. Next, to avoid the influence of impurities or trace moisture introduced by exposing Pt/C to air, we injected different volumes $V_{D_2SO_4/D_2O}$: $V_{H_2SO_4/H_2O}$ = 1:0, 3:1, 2:1, 1:1, 1:2, 1:3, 0:1) of pure O_2-saturated 0.5 M H_2SO_4/H_2O into the same system in situ under the condition of O_2 partial pressure of 1, to obtain the change of OCP with different volume ratios of D_2SO_4/D_2O and H_2SO_4/H_2O. In addition, OCP at different O_2 partial pressures (P_{O_2}/P_0 = 1/3, 1/2, 2/3, 1) in 9 mL of pure 0.5 M H_2SO_4/H_2O were recorded in the same way.

Characterization.

Transmission electron microscope (TEM) images of Commercial Pt/C were recorded on JEM 2100F (JEOL, Japan) with an aberration corrector operated at 200 kV. Small amounts of the catalyst were suspended in ethanol and then placed on a grid before drying.

The concentration of Pt ions in the solution was examined utilizing an inductively coupled plasma mass spectrometer (ICAP QC) from ThermoFisher Scientific. To more intuitively observe the trend of Pt ion concentration in the solution and to mitigate the error due to the minimal amount of material, 500 μL of catalyst ink was dropped onto a 2 cm*2 cm hydrophilic carbon paper (which has been subjected to a soaking process in anhydrous ethanol for a duration of 12 hours, followed by multiple rinses using deionized water), achieving a platinum loading of 50 μg_{Pt} cm^{-2}. The electrode was then infrared heated for a few seconds using an infrared irradiator to increase the adhesion between the catalyst and the conductive carbon paper. Subsequently, the electrode was placed in 150 ml of O_2-free 0.1 M $HClO_4$ for OCP testing, and when the OCP did not change with

time, pure O_2 was introduced into the electrolyte, followed by 46 h of OCP testing. During this testing period, 5 ml of the electrolyte and 5 ml of O_2-saturated fresh electrolyte were withdrawn and re-added sequentially at each time point of 0 h (serving as a baseline), 1 h, 4 h, 10 h, 22 h, and 46 h, respectively. The 5 ml of electrolyte was utilized for ICP detection, while the 5 ml of O_2-saturated fresh electrolyte was employed to ensure the stability of the test system. It is important to note that the data obtained in the subsequent stages have been adjusted to account for this process. This ensures the accuracy and reliability of the experimental results.

Calculations

Calibration of reference electrode.

To accurately calibrate the potentials from *E* vs. Hg/Hg_2SO_4 to *E* vs. RHE, the potentials were experimentally calibrated for the different systems (Eq. S1). Prior to each experimental calibration, the solution was purged with H_2 for 15 min. Then, a rotating Pt disk electrode (Area: 0.19625 cm^2) was used to cycle through the potential range of hydrogen evolution and oxidation to obtain stable the cyclic voltametric (CV) curves at a scan rate of 10 mV s^{-1} under 1600 rpm. Finally, E_{offset} was obtained by averaging the two voltage intercepts at zero current on the CV curve.

$$E_{\mathrm{RHE}} = E_{\mathrm{measured}} - E_{\mathrm{offset}} \quad \text{Eq. S1}$$

Where E_{measured} is E vs. Hg/Hg_2SO_4; E_{offset} is the experimentally determined conversion factor, which represents the potential difference between E vs. Hg/Hg_2SO_4 and E vs. RHE.

Coverage of Pt and Pt oxides.

The potential dependent coverage of Pt can be calculated by the formula:

$$\theta_{\mathrm{Pt}}|_{E=a\ \mathrm{V/b\ mV\ s^{-1}}} = 1 - \frac{Q_{\mathrm{PtO}}|_{E=a\ \mathrm{V/b\ mV\ s^{-1}}}}{\mathrm{Q_T}|_{\mathrm{b\ mV\ s^{-1}}}} \quad \text{Eq. S2}$$

where $\theta_{\mathrm{Pt}}|_{E\ =\ \mathrm{a\ V/b\ mV\ s^{-1}}}$ is the Pt coverage at the potential of a V and the scan rate of b mV s^{-1}; For $Q_{\mathrm{PtO}}|_{E\ =\ \mathrm{a\ V/b\ mV\ s^{-1}}}$, there are two cases. For the anodic scan, it represents the accumulated charge when Pt is oxidized to a V at a scan rate of b mV s^{-1}. For the cathodic scan, it represents the total reduction charge minus the charge of reducing the oxidized Pt to a V at a scan rate of b mV s^{-1}; $\mathrm{Q_T}|_{\mathrm{b\ mV\ s^{-1}}}$ is the total charge of the Pt oxidation/reduction at the scan rate of b mV s^{-1}. For electrochemical testing of different E_{upl}, the coverage of Pt at 0.4 V vs. RHE (1.17 V vs. RHE) is

assumed to be 1 (0) during cathodic or anodic scanning, so that:

$$Q_{\mathrm{PtO}}|_{E=0.4\ \mathrm{V}/10\ \mathrm{mV\ s^{-1}}} = 0 \qquad \text{Eq. S3}$$

$$Q_{\mathrm{PtO}}|_{E=1.17\ \mathrm{V}/10\ \mathrm{mV\ s^{-1}}} = Q_{\mathrm{T}}|_{10\ \mathrm{mV\ s^{-1}}} \qquad \text{Eq. S4}$$

which is used as a basis for calculating the coverage of Pt at a certain potential during the testing of different E_{upl}. For electrochemical testing at different scan rates, the coverage of Pt at 0.4 V vs. RHE (1.07 V vs. RHE) is assumed to be 1 (0) at 10 mV s^{-1} during cathodic or anodic scanning, so that:

$$Q_{\mathrm{PtO}}|_{E=0.4\ \mathrm{V}} = 0 \qquad \text{Eq. S5}$$

$$Q_{\mathrm{PtO}}|_{E=1.07\ \mathrm{V}/10\ \mathrm{mV\ s^{-1}}} = Q_{\mathrm{T}}|_{10\ \mathrm{mV\ s^{-1}}} \qquad \text{Eq. S6}$$

which is used as a basis for calculating the coverage of Pt at a certain potential during the testing of different scan rates.

Number of electron transfer.

$$E_{\mathrm{ORR}}^{\mathrm{eq}} = E^{\theta} + \frac{RT}{\mathrm{n}F}\ln\frac{\mathrm{a}_{(\mathrm{H^+/D^+})}P_{\mathrm{O_2}}^{\frac{1}{4}}}{\mathrm{a}_{(\mathrm{H_2O/D_2O})}^{\frac{1}{2}}}$$

$$= E^{\theta} + \frac{RT}{\mathrm{n}F}\ln\mathrm{k}_1 + \frac{1}{4}\ln\left(P_{\mathrm{O_2}}\right) \qquad \text{Eq. S7}$$

$$= \mathrm{k}_2 + \frac{RT}{4\mathrm{n}F}\ln\left(P_{\mathrm{O_2}}\right)$$

The theoretical equilibrium potential for ORR is given by the Nernst equation. Where E^{θ}= 1.229 V_{NHE} is the standard equilibrium potential, $\mathrm{a}_{(\mathrm{H^+/D^+})}$ is the activity of protons or deuterium ions in solution, $P_{\mathrm{O_2}}$is the dimensionless O_2 pressure, $\mathrm{a}_{(\mathrm{H_2O/D_2O})}$is the activity of water or heavy water, *R* is the ideal gas constant, *T* is the Kelvin temperature, and *F* is the Faraday constant.

$$\mathrm{k}_1 = \frac{\mathrm{a}_{(\mathrm{H^+/D^+})}}{\mathrm{a}_{(\mathrm{H_2O/D_2O})}^{\frac{1}{2}}} \qquad \text{Eq. S8}$$

$$\mathrm{k}_2 = E^{\theta} + \frac{RT}{\mathrm{n}F}\ln\mathrm{k}_1 \qquad \text{Eq. S9}$$

$E_{\mathrm{ORR}}^{\mathrm{eq}}$ is linearly related to $\ln(P_{\mathrm{O_2}})$, other terms being equal.

Mass-tansfer corrected Tafel slope.

$$j_{\mathrm{lim}} = \frac{i_{\mathrm{lim}}}{A} = 0.62nFD^{2/3}\omega^{1/2}v^{-1/6}c_{\mathrm{O_2}} \quad \text{Eq. S10}$$

The Levich equation describes the relationship between the diffusion-limited current and the rotation rate in RDE measurements. j_{lim} and i_{lim} are diffusion-limited current density and current, respectively. A is the geometric area of the electrode, n is the electron transfer number, *F* is Faraday's constant, *D* is the diffusivity, *ω* is the rotation rate, *v* is the kinematic viscosity, and $c_{\mathrm{O_2}}$ is the bulk O_2 concentration.

$$\frac{1}{j_{\mathrm{m}}} = \frac{1}{j_{\mathrm{k}}} + \frac{1}{j_{\mathrm{lim}}} \quad \text{Eq. S11}$$

Koutecký-Levich equation. j_{m}, j_{k}, and j_{lim} are measured current density, kinetic current density, and diffusion-limited current density.

After i-R correction as well as background correction, the kinetic densities at different potentials are obtained by the above equations, and then plotted in terms of the logarithm of the kinetic current densities and the iR-corrected potentials to finally obtain the Mass-transfer corrected Tafel slope.

Kinetic inverse effect.

$$\mathrm{KIE} = \frac{j^{\mathrm{H}}}{j^{\mathrm{D}}}\frac{c_{\mathrm{O_2}}^{\mathrm{D}}}{c_{\mathrm{O_2}}^{\mathrm{H}}} = \frac{1}{0.908}\frac{j^{\mathrm{H}}}{j^{\mathrm{D}}} = 1.101\frac{j^{\mathrm{H}}}{j^{\mathrm{D}}} \quad \text{Eq. S12}$$

The H/D KIE is defined as the ratio of the measured kinetic current density in H_2O (j^{H}) and D_2O (j^{D}), respectively, after iR correction, at given potentials based on the Koutecký–Levich equation. $c_{\mathrm{O_2}}^{\mathrm{H}}$ and $c_{\mathrm{O_2}}^{\mathrm{D}}$ are O_2 solubility in H_2O (1.269×10^{-3} M) and D_2O (1.397×10^{-3} M) at 25 °C and 1 bar.

Thermodynamic equilibrium potential of reactions.

Oxygen Evolution Reaction/Oxygen Reduction Reaction:

$$\mathrm{O_2} + 4\mathrm{H^+} + 4\mathrm{e^-} \rightleftarrows 2\mathrm{H_2O},\ \mathrm{E^\theta} = 1.229 - 0.0591\mathrm{pH} \quad \text{Eq. S13}$$

Pt (Oxide) Oxidation/Pt Oxide Reduction:

$$Pt + H_2O \rightleftarrows PtO + 2H^+ + 2e^-, E^\theta = 0.980 - 0.0591pH$$ Eq. S14

$$PtO + H_2O \rightleftarrows PtO_2 + 2H^+ + 2e^-, E^\theta = 1.045 - 0.0591pH$$ Eq. S15

$$Pt + 2H_2O \rightleftarrows PtO_2 + 4H^+ + 4e^-, E^\theta = 1.000 - 0.0591pH$$ Eq. S16

Pt (Oxide) Dissolution/Pt deposition:

$$Pt \rightleftarrows Pt^{2+} + 2e^-, E^\theta = 1.188 + 0.0295\log(Pt^{2+})$$ Eq. S17

$$PtO_2 + 4H^+ + 2e^- \rightleftarrows Pt^{2+} + 2H_2O, E^\theta = 0.837 - 0.1182pH - 0.0295\log(Pt^{2+})$$ Eq. S18

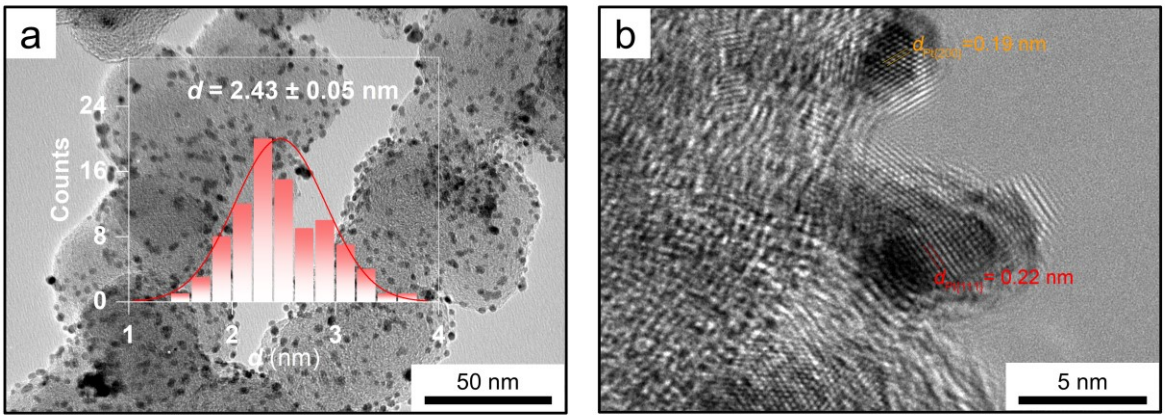

Fig. S1 (a) Regular and (b) high resolution TEM images of commerical Pt/C. The inset is the histrogram of diameters of Pt nanoparticles. The d spacing of 0.22 nm and 0.19 nm can be attributed to the distance of Pt{111} and Pt{200}.

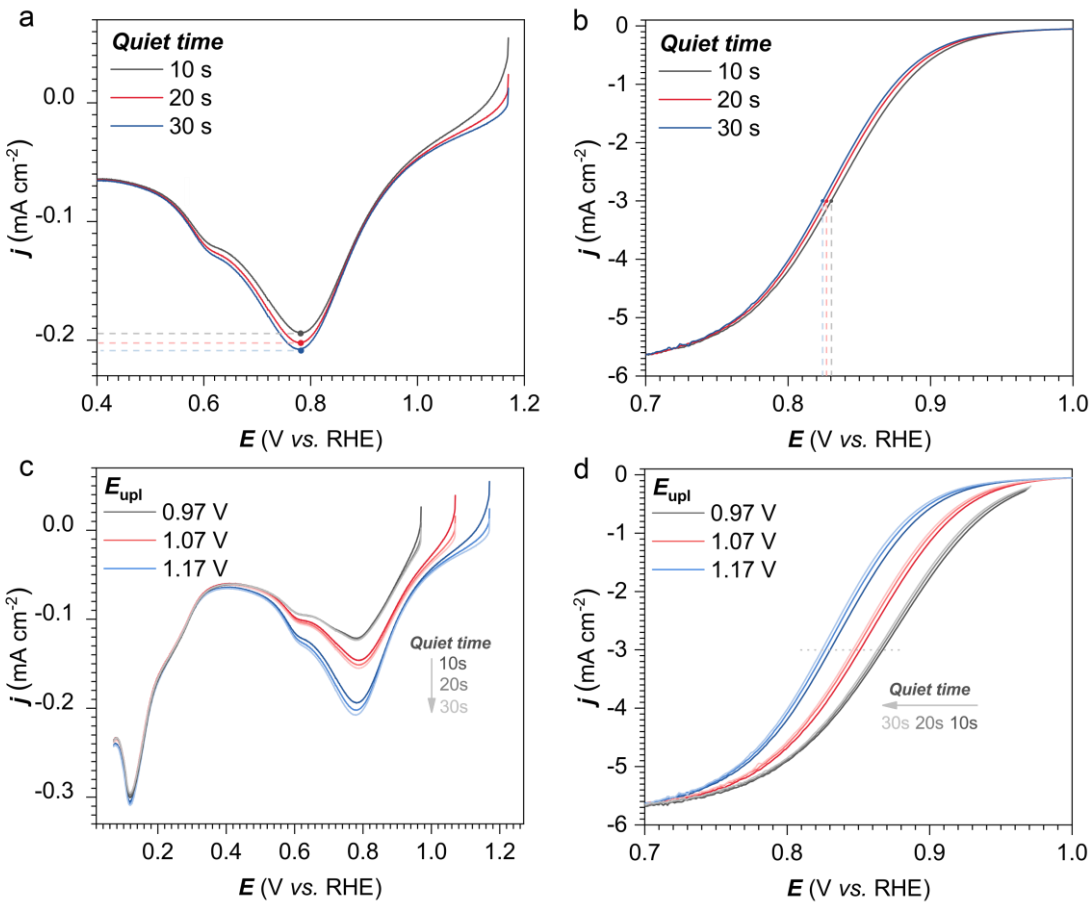

Fig. S2 Quiet time effect on the LSV curves in (a) O_2-free and (b) O_2-saturated electrolytes at 1600 rpm at the scan rate 10 mV s^{-1} in 0.1 M $HClO_4$. Effect of Quiet time on LSV curves in (c) O_2-free and (d) O_2-saturated electrolytes at 1600 rpm at different E_{upl}.

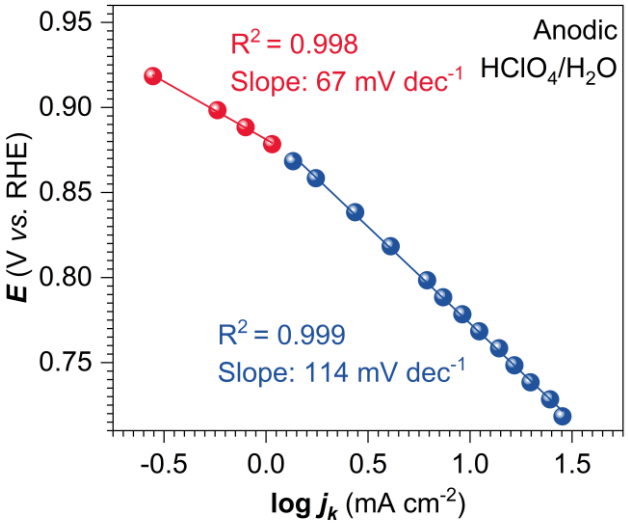

Fig. S3 Mass-transfer corrected Tafel plots for oxygen reduction reaction 0.1 M $HClO_4$.

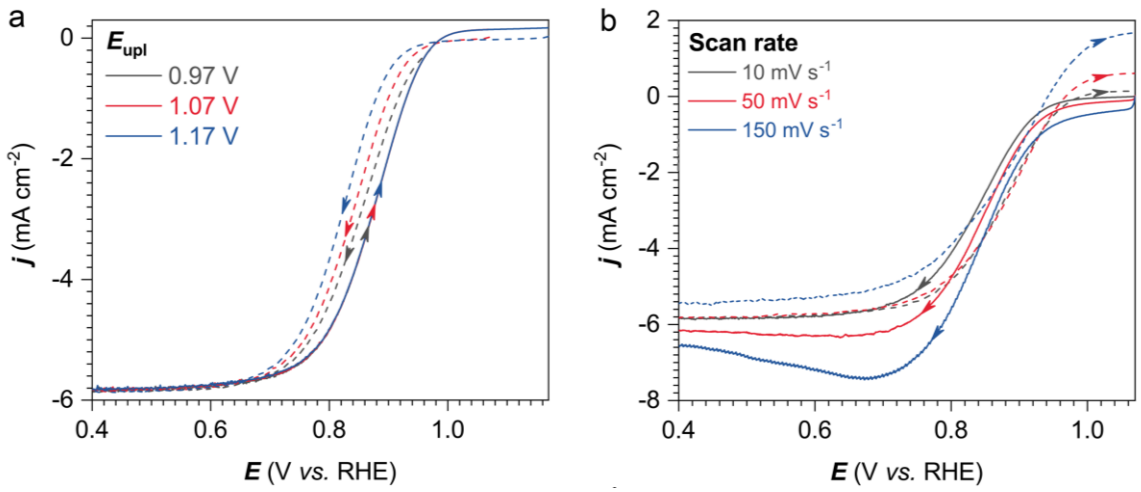

Fig. S4 (a) The cathodic and anodic scans with different E_{upl} in O_2-saturated 0.1 M $HClO_4$ electrolyte at 1600 rpm at the scan rate of 10 mV s^{-1}. (b) The cathodic and anodic scans with different scan rates in O_2-saturated 0.1 M $HClO_4$ electrolyte at 1600 rpm at different scan rates.

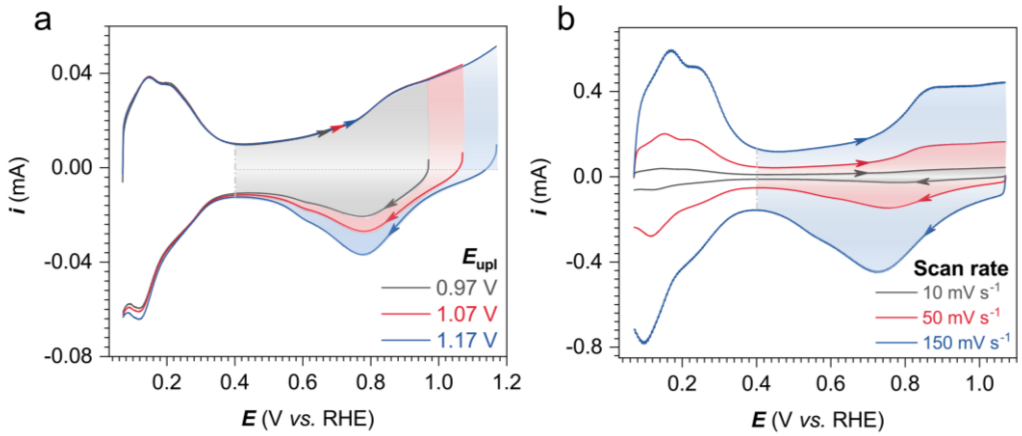

Fig. S5 (a) The cathodic and anodic scans with different E_{upl} in O_2-free 0.1 M $HClO_4$ electrolyte at 1600 rpm at the scan rate of 10 mV s^{-1}. (b) The cathodic and anodic scans with different scan rates in O_2-free 0.1 M $HClO_4$ electrolyte at 1600 rpm at different scan rates. The shaded area in different colors was the integral charge for calculating the proportion of surface Pt oxide.

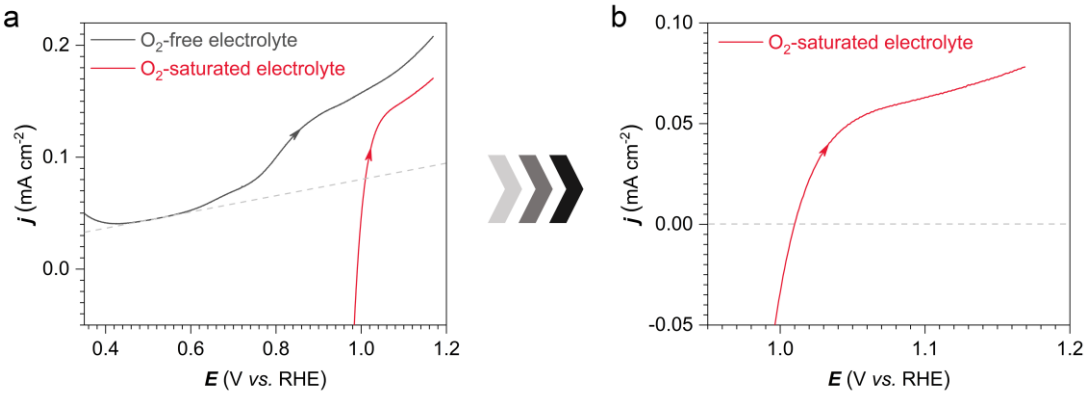

Fig. S6 (a) The anodic scans in O_2-saturated (red) and O_2-free (grey) 0.1 M $HClO_4$ electrolyte at 1600 rpm at the scan rate of 10 mV s^{-1}. (b) the background-corrected anodic scans in O_2-saturated 0.1 M $HClO_4$ electrolyte at 1600 rpm at the scan rate of 10 mV s^{-1}. It is obtained by subtraction of the dashed line (as the double layer capacitance current) from the red curve in (a).

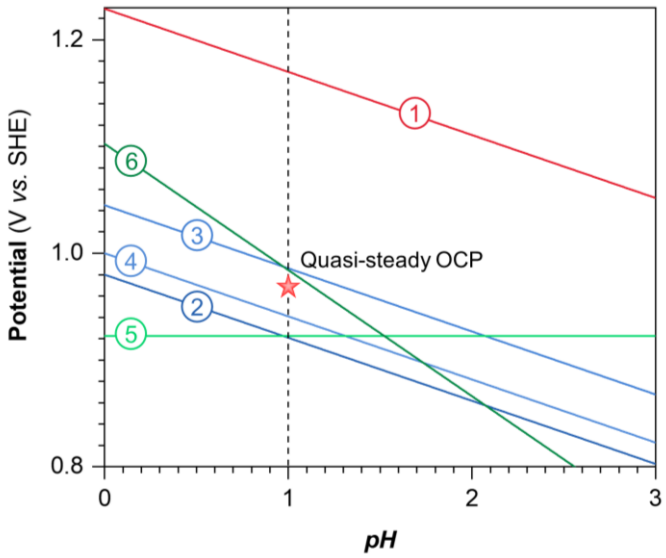

Fig. S7 Pourbaix diagram of Pt and O_2 in water solution. The lines 1-6 correspond to the equilibrium reactions given by Eq. S13-S18.

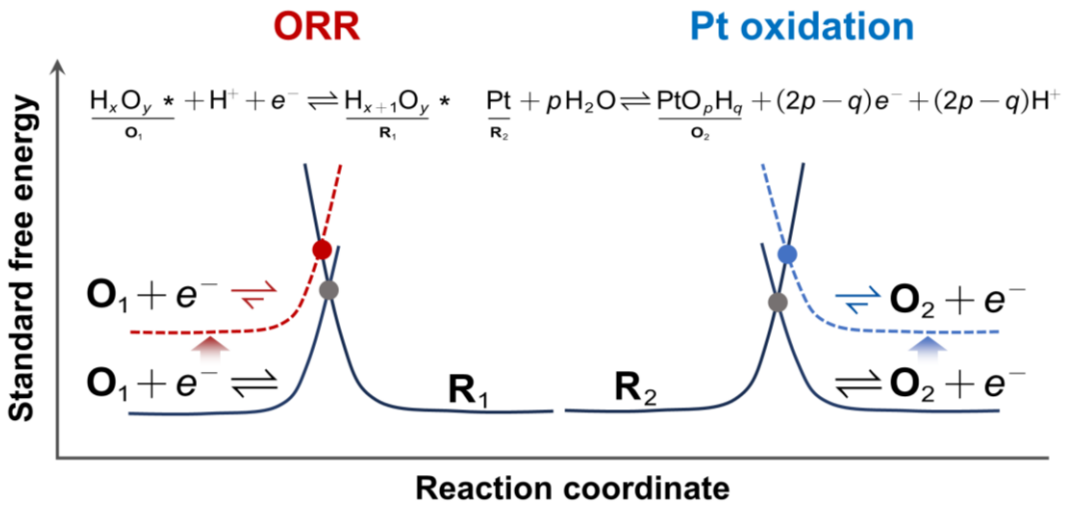

Fig. S8 Effect of the decrease of the applied potential on the redox reactions of O_2 and Pt. The difference in standard free energy between the state at the intersection point and the state at the initial point represents the activation energy of the oxidation/reduction reaction. Where H_xO_y* represents the oxidized species of an elementary reaction step in the ORR and $H_{x+1}O_y$* represents the reduced species of an elementary reaction step in the ORR. PtO_pH_q is the oxidized product of Pt.

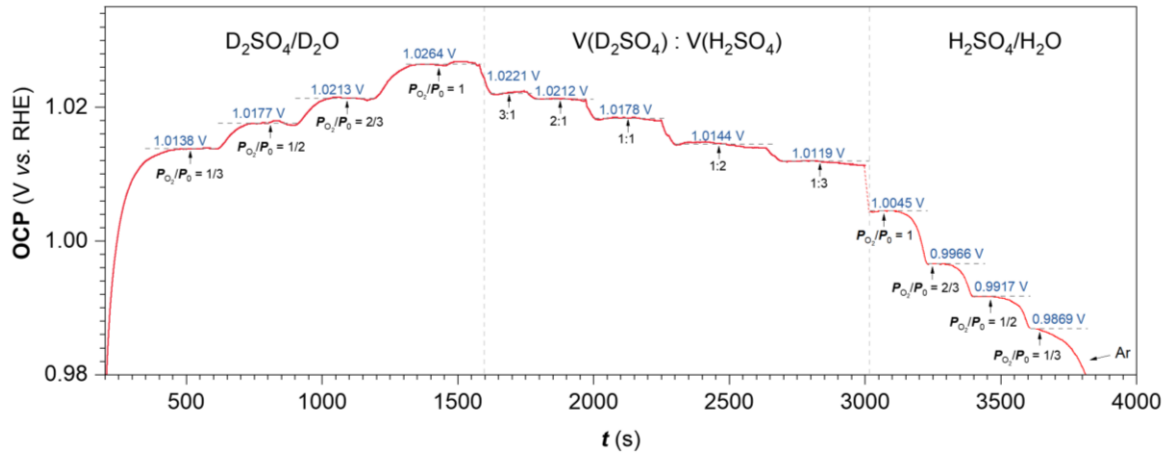

Fig. S9 The partial pressure of O_2 effect on the OCP in 0.5 M H_2SO_4/H_2O and 0.5 M D_2SO_4/D_2O and the volume ratio of D_2SO_4/D_2O to H_2SO_4/H_2O effect on the OCP in O_2-saturated electrolyte.

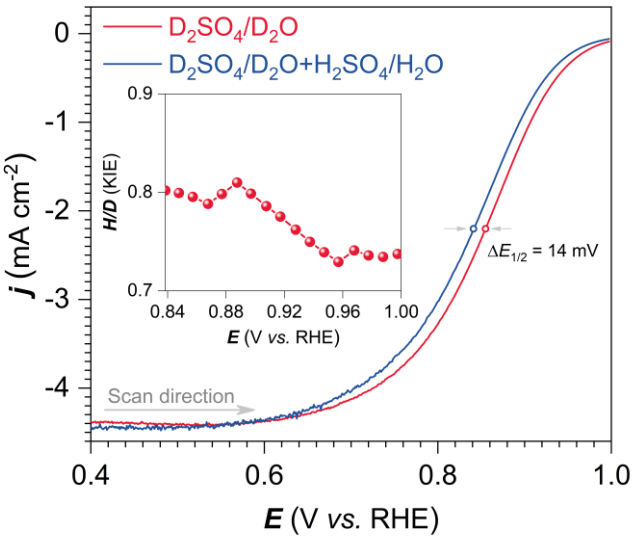

Fig. S10 The anodic LSV curves of Pt/C in O_2-saturated 0.5 M H_2SO_4/H_2O and 0.5 M D_2SO_4/D_2O electrolytes at the scan rate of 10 mV s^{-1}. The inset is the H/D kinetic inverse effect based on the kinetic current density extracted from the Koutecký–Levich equation.

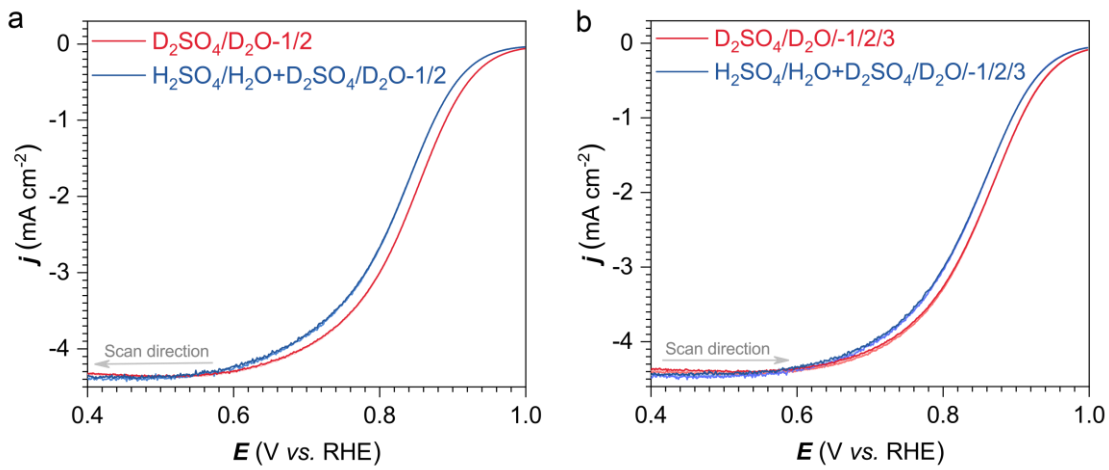

Fig. S11 The cathodic (a) and anodic (b) LSV curves of Pt/C obtained in two individual experiments in O_2-saturated 0.5 M H_2SO_4/H_2O and 0.5 M D_2SO_4/D_2O electrolytes at the scan rate of 10 mV s^{-1}.

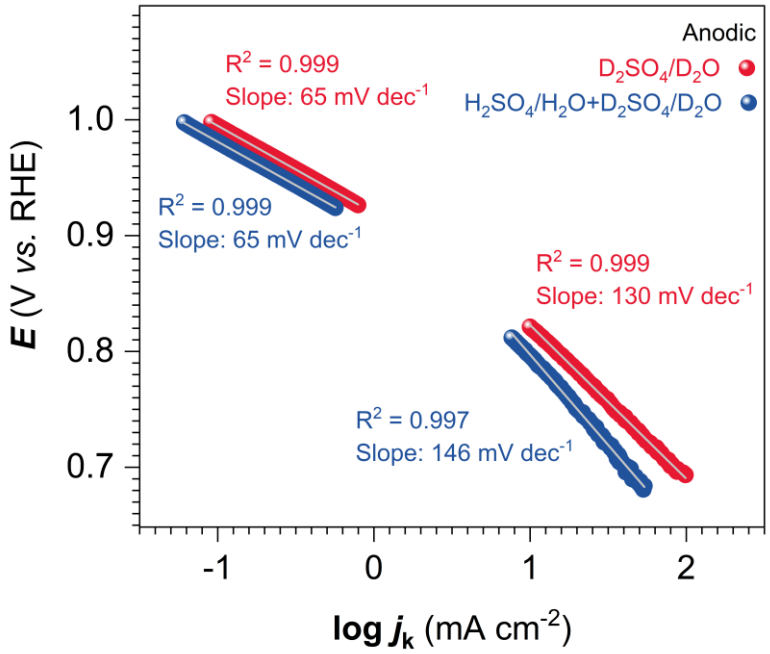

Fig. S12 Mass-transfer corrected Tafel plots (extracted from **Fig. S9**) for oxygen reduction reaction 0.5 M H_2SO_4/H_2O+0.5 M D_2SO_4/D_2O (blue) and 0.5 M D_2SO_4/D_2O (red) electrolytes.

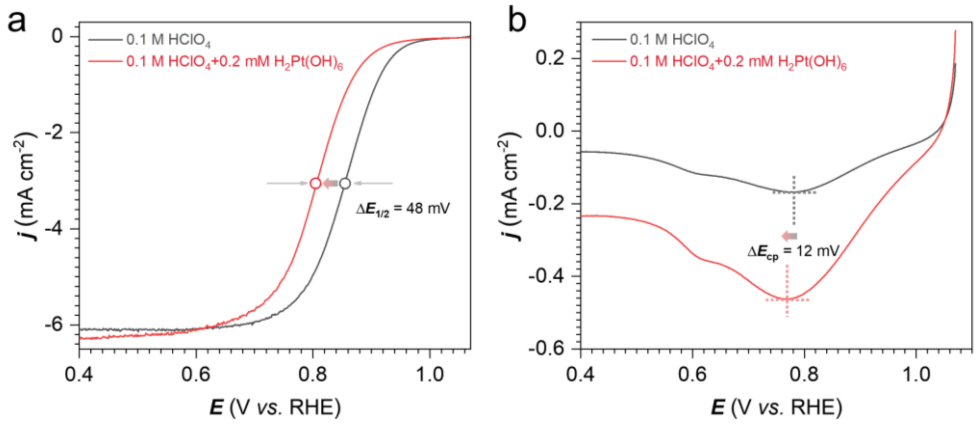

Fig. S13 Effect of $H_2Pt(OH)_6$ on LSV curves obtained in (a) O_2-saturated and (b) O_2-free 0.1 M $HClO_4$ electrolytes at 1600 rpm at the scan rate of 10 mV s^{-1}.

Table S1 Electrochemical performance of materials from the selected publications.

Target material	Reference material	Potential from CV/LSV curve		Electrolytes	Journal
		$E_{cp\text{-}target}/E_{cp\text{-}reference}$ @scan rate	$E_{1/2\text{-}target}/E_{1/2\text{-}reference}$ @scan rate		
Pd@Pt	Pt/C	0.8155/0.7485 50 mV s^{-1}	0.9259/0.9086 10 mV s^{-1}	0.1 M $HClO_4$	Journal of the American Chemical Society[1]
TiNiN@Pt	Pt/C	0.8830/0.7949 50 mV s^{-1}	0.8947/0.8385 10 mV s^{-1}	0.1 M $HClO_4$	Journal of the American Chemical Society[2]
PtPb/C	Pt/C	0.8134/0.7865 50 mV s^{-1}	0.9546/0.8072 10 mV s^{-1}	0.1 M $HClO_4$	Science[3]
Pd@$Pt_{2.7L}$	Pt/C	0.8599/0.7520 50 mV s^{-1}	0.9061/0.8767	0.1 M $HClO_4$	Nature Communication[4]
Pt_3Ni(111)	Pt(111)	0.8469/0.7944	0.9227/0.8624	0.1 M $HClO_4$	Science[5]
NPG-Pd-Pt	Pt/C	0.7255/0.6765 50 mV s^{-1}	0.8918/0.8477 10 mV s^{-1}	0.1 M $HClO_4$	Nature Energy[6]
Pt-PdCo@Pd/C	PdCo@Pd/C	0.7883/0.7396 50 mV s^{-1}	0.8889/0.8629 5 mV s^{-1}	0.1 M $HClO_4$	Journal of the American Chemical Society[7]
fct-FePt/C	Pt/C	0.4661/0.3774 50 mV s^{-1}	0.5329/0.5288 5 mV s^{-1}	0.5 M H_2SO_4	Journal of the American Chemical Society[8]
1D PtNi	Pt/C	0.7643/0.7356 50 mV s^{-1}	0.9631/0.8359 10 mV s^{-1}	0.1 M $HClO_4$	Advanced Materials[9]
J-PtNWs	Pt/C	0.8431/0.7283 100 mV s^{-1}	0.9382/0.8659 20 mV s^{-1}	0.1 M $HClO_4$	Science[10]
Pt-NC	Pt/C	0.8888/0.7478 50 mV s^{-1}	0.9176/0.8832 10 mV s^{-1}	0.1 M $HClO_4$	Science[11]
Pt skin	Polycrystalline Pt	0.8168/0.7873 50 mV s^{-1}	0.8905/0.8482	0.1 M $HClO_4$	Nature Materials[12]

Target material	Reference material	Potential from CV/LSV curve		Electrolytes	Journal
		$E_{cp\text{-}target}/E_{cp\text{-}reference}$ @scan rate	$E_{1/2\text{-}target}/E_{1/2\text{-}reference}$ @scan rate		
Pt(111)-AC	Pt(100) after cycled	0.7494/0.5714 50 mV s^{-1}	0.8985/0.8281 20 mV s^{-1}	0.1 M $HClO_4$	Energy & Environmental Science[13]
Pt(111)	Pt(100)	0.8009/0.5870	0.8488/0.8022 50 mV s^{-1}	0.1 M $HClO_4$	Nature Energy[14]
Pd_cPt_3	Pd_0Pt_1	0.7878/0.7818 50 mV s^{-1}	0.8901/0.8686 10 mV s^{-1}	0.1 M $HClO_4$	Journal of the American Chemical Society[15]
np-NiPt+[MTBD][beti]	np-NiPt	0.7602/0.7423 50 mV s^{-1}	0.9997/0.9681 10 mV s^{-1}	0.1 M H_2SO_4 0.1 M $HClO_4$	Nature Materials[16]
Pt(111)+THA^+	$HClO_4$	0.8087/0.7951 50 mV s^{-1}	0.9066/0.8569 10 mV s^{-1}	0.1 M $HClO_4$	Nature Communication[17]
Pt(111) in CsOH	LiOH	0.7823/0.7292 50 mV s^{-1}	0.9131/0.8165 50 mV s^{-1}	0.1 M CsOH 0.1 M LiOH	Nature Chemistry[18]
Cu/Pt(111)	Pt(111)	0.9451/0.7858 50 mV s^{-1}	0.9036/0.8647 50 mV s^{-1}	0.1 M $HClO_4$	Journal of the American Chemical Society[19]
Pt(111)-CN	Pt(111)	0.8523/0.7876 50 mV s^{-1}	0.8738/0.8523 50 mV s^{-1}	0.05 M H_2SO_4	Nature Chemistry[20]

Supplementary References

1. X. Wang, M. Vara, M. Luo, H. Huang, A. Ruditskiy, J. Park, S. Bao, J. Liu, J. Howe, M. Chi, Z. Xie and Y. Xia, *J. Am. Chem. Soc.*, 2015, **137**, 15036-15042.
2. X. Tian, J. Luo, H. Nan, H. Zou, R. Chen, T. Shu, X. Li, Y. Li, H. Song, S. Liao and R. R. Adzic, *J. Am. Chem. Soc.*, 2016, **138**, 1575-1583.
3. L. Bu, N. Zhang, S. Guo, X. Zhang, J. Li, J. Yao, T. Wu, G. Lu, J. Y. Ma, D. Su and X. Huang, *Science*, 2016, **354**, 1410-1414.
4. X. Wang, S.-I. Choi, L. T. Roling, M. Luo, C. Ma, L. Zhang, M. Chi, J. Liu, Z. Xie, J. A. Herron, M. Mavrikakis and Y. Xia, *Nat. Commun.*, 2015, **6**, 7594.
5. V. R. Stamenkovic, B. Fowler, B. S. Mun, G. Wang, P. N. Ross, C. A. Lucas and N. M. Markovic, *Science*, 2007, **315**, 493-497.
6. J. Li, H.-M. Yin, X.-B. Li, E. Okunishi, Y.-L. Shen, J. He, Z.-K. Tang, W.-X. Wang, E. Yücelen, C. Li, Y. Gong, L. Gu, S. Miao, L.-M. Liu, J. Luo and Y. Ding, *Nat. Energy*, 2017, **2**, 17111.
7. D. Wang, H. L. Xin, Y. Yu, H. Wang, E. Rus, D. A. Muller and H. D. Abruna, *J. Am. Chem. Soc.*, 2010, **132**, 17664-17666.
8. J. Kim, Y. Lee and S. Sun, *J. Am. Chem. Soc.*, 2010, **132**, 4996-4997.
9. L. Bu, J. Ding, S. Guo, X. Zhang, D. Su, X. Zhu, J. Yao, J. Guo, G. Lu and X. Huang, *Adv. Mater.*, 2015, **27**, 7204-7212.
10. M. Li, Z. Zhao, T. Cheng, A. Fortunelli, C. Y. Chen, R. Yu, Q. Zhang, L. Gu, B. V. Merinov, Z. Lin, E. Zhu, T. Yu, Q. Jia, J. Guo, L. Zhang, W. A. Goddard, 3rd, Y. Huang and X. Duan, *Science*, 2016, **354**, 1414-1419.
11. L. Zhang, L. T. Roling, X. Wang, M. Vara, M. Chi, J. Liu, S. I. Choi, J. Park, J. A. Herron, Z. Xie, M. Mavrikakis and Y. Xia, *Science*, 2015, **349**, 412-416.
12. V. R. Stamenkovic, B. S. Mun, M. Arenz, K. J. Mayrhofer, C. A. Lucas, G. Wang, P. N. Ross and N. M. Markovic, *Nat. Mater.*, 2007, **6**, 241-247.
13. D. Li, C. Wang, D. S. Strmcnik, D. V. Tripkovic, X. Sun, Y. Kang, M. Chi, J. D. Snyder, D. van der Vliet, Y. Tsai, V. R. Stamenkovic, S. Sun and N. M. Markovic, *Energy Environ. Sci.*, 2014, **7**, 4061-4069.
14. J.-C. Dong, X.-G. Zhang, V. Briega-Martos, X. Jin, J. Yang, S. Chen, Z.-L. Yang, D.-Y. Wu, J. M. Feliu, C. T. Williams, Z.-Q. Tian and J.-F. Li, *Nat. Energy*, 2018, **4**, 60-67.
15. J. X. Wang, H. Inada, L. Wu, Y. Zhu, Y. Choi, P. Liu, W. P. Zhou and R. R. Adzic, *J. Am. Chem. Soc.*, 2009, **131**, 17298-17302.
16. J. Snyder, T. Fujita, M. W. Chen and J. Erlebacher, *Nat. Mater.*, 2010, **9**, 904-907.
17. T. Kumeda, H. Tajiri, O. Sakata, N. Hoshi and M. Nakamura, *Nat. Commun.*, 2018, **9**, 4378.
18. D. Strmcnik, K. Kodama, D. van der Vliet, J. Greeley, V. R. Stamenkovic and N. M. Markovic, *Nat. Chem.*, 2009, **1**, 466-472.
19. I. E. Stephens, A. S. Bondarenko, F. J. Perez-Alonso, F. Calle-Vallejo, L. Bech, T. P. Johansson, A. K. Jepsen, R. Frydendal, B. P. Knudsen, J. Rossmeisl and I. Chorkendorff, *J. Am. Chem. Soc.*, 2011, **133**, 5485-5491.
20. D. Strmcnik, M. Escudero-Escribano, K. Kodama, V. R. Stamenkovic, A. Cuesta and N. M. Markovic, *Nat. Chem.*, 2010, **2**, 880-885.